Development of Self-adaptive Digital Twin for Battery Monitoring and Management System

Kun Fu
School of Engineering and Design
Technical University of Munich
Munich, Germany
kun.fu@tum.de

Thomas Hamacher
School of Engineering and Design
Technical University of Munich
Munich, Germany
thomas.hamacher@tum.de

Vedran S Perić
School of Engineering and Design
Technical University of Munich
Munich, Germany
vedran.peric@tum.de

***Abstract*—The application of digital twin (DT) on battery energy storage systems (BESS) has attracted increasing attention in the last decade. However, existing studies usually focus on building pre-calibrated DT for state estimation and prediction. These DTs lack the ability for dynamic adaptation to changes in battery aging and evolving operating environment, which thus limits their effectiveness in intelligent decision-making for system performance enhancement. Therefore, this work develops a self-adaptive DT for battery monitoring and management system (DT-BMMS). The proposed self-adaptive algorithm ensures accurate long-term mapping between the physical entity and the digital model. Additionally, a model predictive control-based state-of-charge (SOC) balancing method is deployed. Simulation results demonstrate the capability of the developed DT-BMMS to adaptively adjust the DT as the system evolves, which allows the maintenance of SOC balancing under different scenarios.**

***Index Terms*—Battery SOC equalization, digital twin, equivalent circuit model, extended Kalman filter, model predictive control, self-adaptive modeling**

I. INTRODUCTION

In the era of Industry 4.0, with the rise of technologies such as big data, Internet of Things, blockchain, and artificial intelligence, digital twin (DT) has gained increasing attention [1]. As a precise, self-adaptive, and dynamic digital duplication of the physical entities, DT integrates real-time data, digital model, and advanced management algorithms to improve the understanding and performance of the physical entity [2]. After being initially introduced by Grieves et al. in 2003 [3] and subsequently embraced by NASA [4], it has entered into a phase of rapid development, with applications extended to diverse domains, including power and energy systems. By combining real-time data with digital models, power and energy equipment can be better cooperated and controlled, resulting in higher efficiency and lower cost.

Battery energy storage system (BESS) is an important part of modern power systems, not only powering electric vehicles (EVs), but also offering flexibility for the grid. As an iconic application, DT for battery monitoring and management system (DT-BMMS) has been proved to improve BESS performance through accurate state monitoring and intelligent decision-making. Semeraro et al. [5] proposed guidelines for DT development, which capture the behavior and characteristics of the BESS to monitor and optimize the system behavior. Naguib et al. [6] reviewed the state-of-charge (SOC) estimation methods, where the battery equivalent circuit model (ECM) and extended Kalman filter (EKF) are discussed. Apart from that, authors of [7] utilized DT to monitor battery temperature and visualized the digital model with a user interface. To further enhance system operational performance, Qu et al. [8] developed a deep learning-based DT model for lithium-ion battery and applied long short-term memory to forecast battery performance degradation. Besides, advanced control and management methodologies were also used in DTs. To prolong the life of the battery, varieties of DT-based SOC balancing techniques were discussed in [9]. Authors of [10] explored the potential of applying model predictive control (MPC)-based battery DT in peak shaving scenario. And the authors of [11] reviewed the EV powering application, where advanced management methods, like battery passport, are integrated with DT to decrease the cost at the life-cycle level. To release the computation and data storage limitations of the onboard devices, cloud assisted technology was discussed in [12] and [13] to improve the performance of BESS through SOC balancing. In the studies mentioned above, a variety of advanced model-based state monitoring and controlling methods were utilized. However, their accuracy is highly dependent on the DT models, where the pre-calibrated models exhibit limited accuracy in uncertain environment.

Therefore, considering the challenge of DT inaccuracy, there is a need to find a self-adaptive modeling algorithm and an effective decision-making strategy for DT-BMMS [14]. This paper develops a self-adaptive battery DT to monitor the battery SOC, meanwhile maintain SOC balancing. Leveraging the system knowledge within the DT, MPC is selected as the real-time controller with its ability to optimize system behavior over a predictive horizon under various constraints and environments [15-17]. In order to demonstrate the versatility of the developed DT-BMMS, two prevalent battery applications are considered: EV powering and power system peak shaving, which represent high-dynamic and low-dynamic BESS usage scenarios, respectively. Fig. 1 illustrates the overview of the DT-BMMS. The collected data from the physical space are utilized for DT modeling with the self-adaptive particle swarm

optimization (SaPSO) method, establishing the battery DT in the digital space. Additionally, the error integration method is employed to trigger the self-adaptation algorithm. The EKF is then employed to fuse data from both physical and virtual spaces, thus accurately monitoring the SOC of the battery. The ECM and estimated SOC are further utilized by MPC to generate optimal charging and discharging control signals for SOC balancing, thereby enhancing system performance. The robustness of the proposed SaPSO is proved through repeated simulations over different working conditions, and different battery packs of varying scales are tested to prove the scalability of the proposed method.

The main contributions of this work are summarized as follows:

(1) DT-BMMS is developed within a comprehensive digital twin architecture, leveraging an emulated battery platform for simulation and analysis.

(2) A SaPSO algorithm is incorporated into the modeling phase, ensuring long-term accurate mapping of the digital model to the physical entity.

(3) MPC-based cell balancing strategy is applied, enhancing the performance of the system under both high-dynamic and low-dynamic operation scenarios.

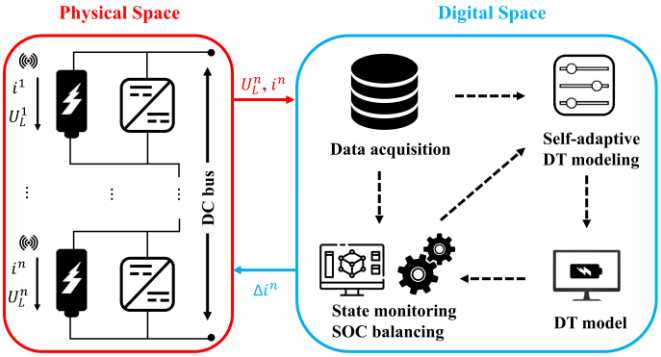

Fig. 1 Overview of the DT-BMMS.

The rest of this paper is structured as follows. In Section II, the comprehensive DT architecture is introduced, upon which the digital models, monitoring, and control algorithms used in DT-BMMS are given in detail. The test scenarios and analysis of the simulation are presented in Section III, and finally, Section IV provides the conclusion.

II. METHODOLOGY

A. Digital twin architecture

The development of DT assembles various modeling, monitoring and management algorithms with a specific target. The comprehensive architecture applied in this paper consists of several components: series-connected battery, self-adaptive DT modeling, DT model, and specific application. The overview of the architecture is shown in Fig. 1, where the battery entity is represented by ECM [18] and the dashed arrows indicate the data flow in digital space. The emulated battery functions as physical space, serving as the foundation upon which the DT is based, capturing the physical attributes, behaviors, and characteristics. The captured voltage and current data are used for self-adaptive DT modeling, enabling a dynamic and accurate digital representation. The digital space allows state monitoring, prediction and analysis in a controlled and risk-free environment. The generated current control signal is then fed back to the battery to improve its performance. In the following sections, the detailed ECM model, SaPSO method, SOC monitoring and balancing algorithms under different scenarios will be introduced.

B. Battery model

Currently, there are three mainstream approaches with respective advantages and limitations for battery modeling: electrochemical model, ECM, and data-driven model [19]. This study makes use of the ECM approach as Fig. 2 shows. ECM is a grey-box model utilizing a combination of resistor, capacitor and voltage source to characterize the dynamic response of the battery, and utilizing the collected data to tune the corresponding parameters. Due to the ease of parametrization and implementation, as well as the low computing cost and computational efficiency, it represents a trade-off between accuracy and real-time performance on mirroring a physical battery in digital space [20].

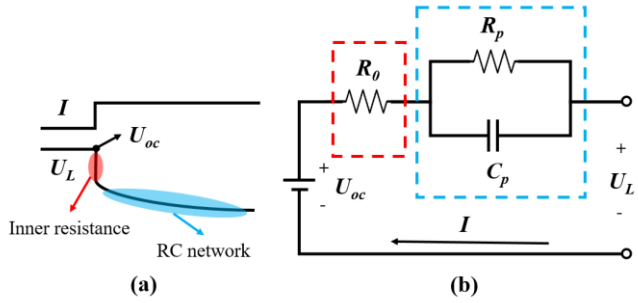

Fig. 2 Schematic of the battery ECM. (a) Factors affecting the battery dynamic response. (b) Circuit diagram of the ECM.

The ECM has a simple mathematical expression, where the dynamics of the charging and discharging process are specified by the following equation set:

$$\frac{dSOC^n}{dt} = -\eta\frac{i^n}{E^n} + \omega_1 \tag{1a}$$

$$\frac{dU_p^n}{dt} = -\frac{U_p^n}{R_p^n C_p^n} + \frac{i^n}{C_p^n} + \omega_2 \tag{1b}$$

$$U_L^n = U_{oc}(SOC^n) - U_p^n - i^n R_0^n + \beta \tag{1c}$$

Where the superscript n denotes the nth cell in the battery module, which consists of a total of N cells; η is the coulombic efficiency of the battery; i is the current and E is the battery capacity in Amp Hour; R_0 is the internal resistance; R_p and C_p are the polarization resistance and capacitance, respectively; U_p and U_L are terminal voltage of the polarization capacitance and the battery cell, respectively; ω_1, and ω_2 are process noise, and β is measurement noise; U_{oc} is the open circuit voltage

Submitted to the 23rd Power Systems Computation Conference (PSCC 2024).

dependent on SOC, which is fitted by a fifth-order polynomial in this paper, resulting in (1c) being nonlinear.

To better suit computer simulation and model-based predictive control, the continuous-time ECM is discretized with sampling time S, as the following equation shows:

$$SOC_{k+1}^n = SOC_k^n - \eta \frac{i_k^n}{E^n} S + \omega_{1,k} \quad (2a)$$

$$U_{p,k+1}^n = U_{p,k}^n e^{-\frac{S}{R_p^n C_p^n}} + R_p^n \left(1 - e^{-\frac{S}{R_p^n C_p^n}}\right) i_k^n + \omega_{2,k} \quad (2a)$$

$$U_{L,k}^n = U_{oc}(SOC_k^n) - U_{p,k}^n - i_k^n R_{0,k}^n + \beta_k \quad (2c)$$

C. Self-adaptive modeling

The parameters of ECM are dynamically updated by the PSO-based system identification block that processes real-time measured data [21]. At the initial stage, parameter identification for the digital model is conducted using the measured battery current and voltage data within one hour. The identified parameters are then applied to the ECM in digital space. Subsequently, the digital space runs in parallel with the physical space.

The R_0, R_p and C_p of ECM are the parameters to be tuned by PSO, and the measured current from physical space is applied as input and the measured voltage is the target value. Therefore, a 3-dimensional search space is explored and the discretized ECM equation is used as the fitness function. The position of each particle is represented by $P_i = (p_{i1}, p_{i2}, p_{i3})^T$. At each iteration, each particle updates its position and records the best solution from all previous generations, denoted as P_{best}. Meanwhile, the overall best solution, denoted as G_{best}, is also recorded. The iteration process is described by the following equations:

$$v_{i+1} = wv_i + c_1 r_1 (P_{best} - P_i) + c_2 r_2 (G_{best} - P_i) \quad (3a)$$

$$P_{i+1} = P_i + v_{i+1} \quad (3b)$$

Where v_i represents the velocity of the ith particle, w is the inertia weighting factor, c_1, c_2 are learning rates and r_1, r_2 are random values between 0 and 1.

The integral area error (IAE) of the difference between the voltage obtained through ECM and measurement is used as the fitness value, as the following equation shows:

$$Min \;\; IAE_U = \int_{t_1}^{t_2} |U_{ECM} - U_{MEA}| \, dt \quad (4)$$

Where t_1 and t_2 represent the start and end time of data measurement, respectively; U_{ECM} and U_{MEA} are voltage obtained through ECM and measurement, respectively; R_0, R_p and C_p obtained after the convergence of PSO is assigned to the ECM in the digital space, yielding the complete ECM model mirroring the battery in the physical space.

The integrated voltage error is further utilized by SaPSO algorithm to dynamically update the parameters of ECM. Based on current access rules for the European electricity market, 15 minutes was selected as the minimum servicing duration under the peak shaving scenario [22]. As a balance between adaptation frequency and output accuracy, 15 minutes is also choice as the length of error integration window. Once the integrated error between the physical and digital space feedback voltages exceeds a threshold, PSO is invoked again to perform adaptive update for the ECM. The detailed algorithm is given as follows, where the estimated voltage and measured voltage of the nth cell are separately represented by $U_{L,ECM}^n$ and $U_{L,MEA}^n$. The threshold is determined by the acceptable error range, which will be introduced in Section III.

Algorithm 1 Error integration-based SaPSO

Initialization
Parameter identification of ECM using PSO
Continuous data collection
Collecting the terminal voltage of nth battery module from both digital ($U_{L,ECM}^n$) and physical ($U_{L,MEA}^n$) spaces
Self-adaptation
Error integration in last 15 minutes with time steps of 1s
$E^n = \int_{t-15}^{t} \left(U_{L,ECM}^n - U_{L,MEA}^n\right) \quad n \in N, \; t \geq 15 \; min$
Trigger:
If $E^n \leq threshold$ **then**
Keep running, and steps 4,7 and 9 are repeated
Else
Self-adaptation with PSO

D. EKF-based state monitoring

The EKF algorithm is an extension of Kalman filter [23] in nonlinear system. It fuses the measured and estimated data to provide reliable results. Compared to the widely used Ampere-hour integration method for SOC calculation, EKF shows robustness against the unknown noise and uncertainties of the system, but relies on the precise system knowledge. Thus, the DT-BMMS provides the EKF with real-time measurements and a dynamically adapted battery model for SOC estimation.

At each time step, the Taylor formula is used to linearize the discrete state space equation of the system. For the battery model shown in (2), it can be written in the form of (5), and the state transition matrix and observation matrix can be obtained through (6).

$$x_{k+1} = f(x_k, u_k) + \omega_k \quad (5a)$$

$$y_k = h(x_k, u_k) + \beta_k \quad (5b)$$

$$\hat{A}_k = \left.\frac{\partial f(x_k, u_k)}{\partial x_k}\right|_{x_k = \hat{x}_k^+}, \quad \hat{C}_k = \left.\frac{\partial h(x_k, u_k)}{\partial x_k}\right|_{x_k = \hat{x}_k^-} \quad (6)$$

Where $u_k = i_k^n$ is the input matrix; $x_k = [SOC_k^n, \;\; U_{p,k}^n]^T$ and $y_k = U_{L,k}^n$ are the state matrix and result matrix; $\omega_k \sim (0, Q_k)$ and $\beta_k \sim (0, R_k)$ separately represent the independent, zero mean, Gaussian process noise and measurement noise with covariance matrices $Q_k = E[\omega_k \;\; {\omega_k}^T]$ and $R_k = E[\beta_k \;\; {\beta_k}^T]$. Combining (2), (5) and (6), the final expression of the state transition matrix and observation matrix are as follows:

$$\hat{A}_k = \begin{bmatrix} 1 & 0 \\ 0 & e^{-\frac{1}{R_p C_p}} \end{bmatrix}, \quad \hat{C}_k = \left[\left.\frac{\partial U_{oc}(SOC)}{\partial SOC}\right|_{SOC = \widehat{SOC}_k^-}, \;\; 1 \right] \quad (7)$$

The EKF algorithm for SOC estimation has two basic steps, namely the prediction step and the update step. Prior estimations are obtained based on the ECM in the prediction stage. In the update stage, the Kalman gain is updated based on

the ECM estimated value and real-time measurements, and then the posterior results are further calculated. For convenience, a summary of the EKF algorithm is given as follows, with the same symbols in (5), (6) and (7):

Algorithm 2 Regression process of EKF in each step

Initialization
Initial state of battery x_0
Prediction step
State estimation:
$\hat{x}_k^- = f(\hat{x}_{k-1}^+, u_{k-1})$
Error covariance:
$P_k^- = \hat{A}_{k-1} P_{k-1}^+ \hat{A}_{k-1}^T + Q_k$
update step
Kalman gain matrix update:
$K_k = P_k^- \hat{C}_k^T (\hat{C}_k P_k^- \hat{C}_k^T + R_k)^{-1}$
State estimation update:
$\hat{x}_k^+ = \hat{x}_k^- + K_k(y_k - h(\hat{x}_k^-, u_k))$
Error covariance update
$P_k^+ = (I - K_k \hat{C}_k P_k^-) P_k^-$

E. MPC-based battery balancing

As one of the most suitable optimal decision-making methods within the DT framework [24], MPC is employed in this study for SOC-based battery balancing, as illustrated in Fig. 3. The optimization objective is to achieve SOC convergence among all series-connected batteries by adjusting the operation currents while satisfying operational requirements. An error band of ± 0.5% plus the average SOC is considered as the criterion for achieving equilibrium [12]. The corresponding optimization problem is described by the following equations:

$$min \quad \mathcal{J}(u_k) = \sum_{t=1}^{M} \sum_{n=1}^{N} (SOC_{k+t}^n|_k - \overline{SOC}_k) \tag{8a}$$

$$s.t. \quad x_{k+t+1}^n|_k = f^n(x_{k+t}^n|_k, \quad u_{k+t}^n|_k) \quad t \in M \tag{8b}$$

$$y_{k+t}^n|_k = h^n(x_{k+t}^n|_k, \quad u_{k+t}^n|_k) \quad t \in M \tag{8c}$$

$$\underline{u} \leq u_{k+t}^n|_k \leq \overline{u} \quad t \in M \tag{8d}$$

$$\underline{y} \leq y_{k+t}^n|_k \leq \overline{y} \quad t \in M \tag{8e}$$

$$\underline{\Delta u} \leq \Delta u_{k+z}^n|_k \leq \overline{\Delta u} \quad z \in Z \tag{8f}$$

$$\Delta u_{k+m}^n|_k = 0 \quad m \in M - Z \tag{8g}$$

$$I_{demand} = \sum_{n=1}^{N} u_{k+z}^n|_k \quad t \in M \tag{8h}$$

Where $\overline{SOC}_k$ is the average SOC at current time step k, and I_{demand} is the current demand in a specific scenario; $\underline{u}$ and $\overline{u}$ separately denote the lower and upper limitations of the control variable, similar for system output y and the changing rate of the control variable Δu; M and Z represent the prediction horizon and control horizon, respectively.

Equation (8) defines the objective function $\mathcal{J}$ as the cumulative error of all battery cells deviating from the average SOC within the prediction horizon. Constraint (8b) to (8e) indicate that the evolution prediction of nth battery has to follow the ECM in the virtual space, meanwhile the control variable and the system output, i.e. the current and the SOC, should be within the specified range. Constraint (8f) and (8g) signify that the changing rate of the control variable should obey the limitations within the control horizon, while they remain unchanged to allow the system to evolve freely beyond that. Finally, constraint (8h) indicates that during the balancing process, the battery should always satisfy the energy demand.

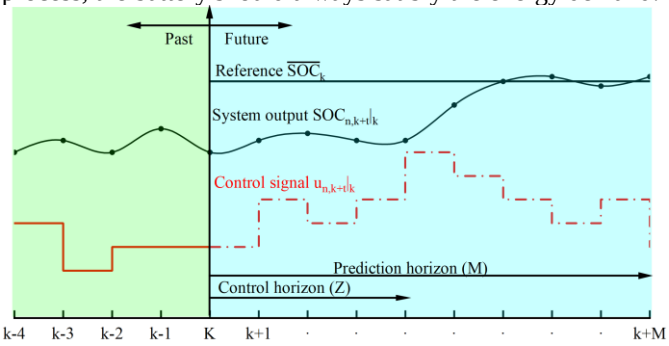

Fig. 3 Scheme of MPC for ***n***th battery module at time point ***k***.

III. SIMULATION AND RESULTS

To validate the effectiveness of the developed self-adaptive DT-BMMS, an emulated battery entity is developed in the Matlab/Simulink environment [18]. The collected current and voltage data are utilized for ECM parameter identification. An S-function is applied to simulate an increase in the battery inner resistance at 1800s, thereby simulating the changes in battery's characteristics caused by the operational environment variations or inherent aging, and validating the effectiveness of the self-adaptation algorithm. It is worth noting that abrupt changes in internal resistance represent an extreme scenario, imposing the system with the highest level of stress. In reality, changes tend to be more gradual, which is considered to pose less of a challenge to system adaptation.

In order to improve the robustness of the PSO, its parameters are carefully selected. From the previous heuristics found [25, 26], four parameters influence the robustness and convergence behavior of PSO, as shown in Table I. On the premise that it is enough to solve the problem, smaller swarm size brings less calculation burden, and proper weighting factor, velocity limitation and learning rate mitigates local optimal problem and accelerates convergence. Following these rules, the finally selected values, determined after trial and error, are provided in Table I. In addition to the appropriate parameters selection, a hundred repeated simulations are also conducted to demonstrate the robustness of the PSO. Randomly generated changes are introduced on internal resistance to activate the SaPSO, where the lower and upper limits are separately set as 20% and 50% based on empirical value [27].

TABLE I PARAMETER SELECTION FOR PSO

Parameters	Empirical values	Selected values
Swarm size	[20,50]	20
Inertia weighting factor	[0.5,1]	0.8
Velocity limitation	position range dependent	[-100,100]
Learning rate	less than 2	0.5

In practical allocations of BESS, tens or even hundreds of battery cells are connected together. To validate the effectiveness and scalability of the SOC balancing method based on MPC, two distinct cases are designed. For the first case, six 18650 cells, detailed parameters listed in Table II [28], are connected in series in the battery module to validate the effectiveness of the proposed method under both high-dynamic and low-dynamic scenarios. Different initial SOC deviations are tested, namely the 10% scenario (100%, 98%, 96%, 94%, 92%, and 90%), and the 25% scenario (100%, 95%, 90%, 85%, 80%, and 75%). Additionally, the inner resistance of each battery is increased by 10%, 20%, 30%, 40%, 50% and 60% respectively, at 1800s, to verify the ability of DT-BMMS to maintain battery equilibrium. For the second case, six modules, each with six cells, are tested to prove the scalability of the proposed method for larger-scale BESS. The modules are respectively set to the mean and standard deviation (SD) of the SOC value of 80% and 0.1, and the cell SOC fluctuates randomly by $\pm 2.5\%$ relative to the module average SOC.

TABLE II PARAMETERS OF 18650 BATTERY

Descriptions	Values
Nominal capacity (Ah)	2
Nominal voltage (V)	3.7
Cutoff charging voltage (V)	4.2
Coulombic efficiency (%)	97
Threshold of integrated voltage error (V/15mins)	16.65

During high-dynamic service provision, the battery operates according to the Beijing Bus Dynamic Stress Test (BBDST) profile [29], with the current changing every few seconds, as shown in Table III. For low-dynamic service provision, the battery adjusts its operating current every 15 minutes, following the profile of -3A, 3A, -6A, 6A in 1 hour. The demand power is proportionally increased in the second case. Fig. 4 depicts the relationship between open circuit voltage and SOC of the 18650-battery cell (left), and the voltage-current profile under BBDST conditions (right). Thus, the accuracy of the EKF algorithm is verified through the comparison between the estimated value and the actual value.

TABLE III BEIJING BUS DYNAMIC STRESS TEST

Step	Current (A)	Step time (s)	Total time (s)	Working conditions
1	-3.4	21	21	Start
2	-6.5	12	33	Accelerate
3	-0.4	16	49	Sliding
4	1.3	6	55	Brake
5	-3.4	21	76	Accelerate
6	-0.4	16	92	Sliding
7	1.3	6	98	Brake
8	-6.5	9	107	Accelerate
9	-8.3	6	113	Rapid accelerate
10	-3.4	21	134	Accelerate
11	-0.4	16	150	Sliding
12	1.3	6	156	Brake
13	-6.5	9	165	Accelerate
14	-8.3	6	171	Rapid accelerate
15	-3.4	21	192	Accelerate
16	-0.4	16	208	Sliding
17	3.1	9	217	Brake
18	1.3	6	229	Brake
19	-0.4	71	300	Parking

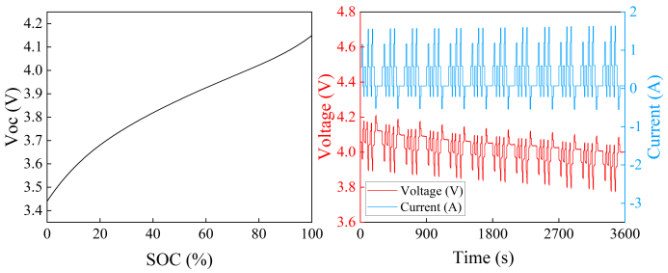

Fig. 4 Left: Voc-SOC curve. Right: U-I profile under BBDST condition.

Following formula gives the optimization problem of MPC:

$$min \quad \mathcal{J} = \int_{t=0}^{T} (X^T \theta X + \Delta u^T \Phi \Delta u) dt \tag{9}$$

Where X is the SOC deviation and Δu is the current change of each cell; θ and Φ are diagonal matrices, tuned to penalize the SOC deviation and the magnitude of current change. Additionally, the prediction horizon M and control horizon Z are carefully considered to balance the efficiency and effectiveness. The selected parameters are listed in Table IV.

TABLE IV PARAMETERS SETTING FOR MPC

Descriptions	Symbols	Values
Sampling time (s)	S	1
Prediction horizon	M	50
Control horizon	Z	20
States weights	θ	5
Input weights	Φ	0.1
Limiation on SOC (%)	$\underline{y}$ / $\overline{y}$	[0, 100]
Limiation on current (A)	$\underline{u}$ / $\overline{u}$	±2
Limiation on current changing rate (A/s)	$\underline{\Delta u}$ / $\overline{\Delta u}$	±2

A. *Results of self-adaptive modeling*

The output voltage generated by both physical and digital spaces under the applied BBDST condition is depicted in the former 1800s in Fig. 5. To simulate changes in battery characteristics [30], the inner resistance of the emulated battery entity is increased by 50% at 1800s, and the simulation results are shown in the latter 1800s of Fig. 5.

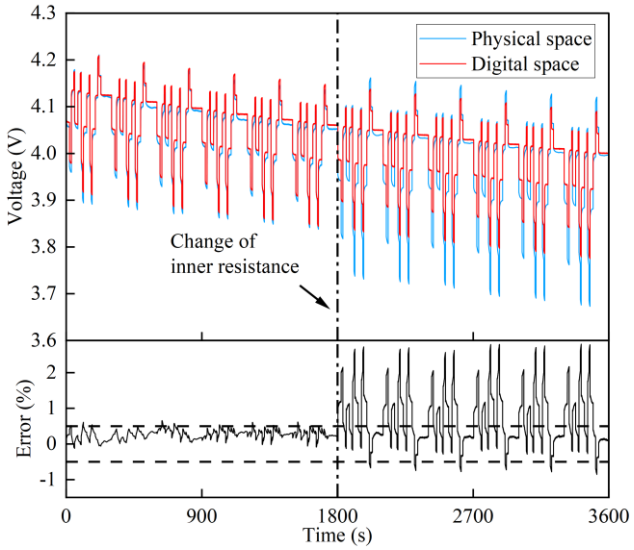

Fig. 5 Voltage output (upper) and absolute error between DT and physical entity (lower) with inner resistance increases at 1800s.

It can be observed that before the change in inner resistance, the ECM identified based on PSO exhibits high accuracy, with voltage errors remaining within 0.5% most of the time. As shown in (10), the threshold for the integrated voltage error over the last 15 minutes is determined based on this value. Where 3.7V is the nominal voltage, 900s is the length of integration range.

$$Threshold = 0.5\% * 3.7 * 900 = 16.65\ (V/15min) \quad (10)$$

After the change in inner resistance at 1800s, the digital space outputs mismatched with the physical space outputs. This is evident in Fig. 6, where two cases are tested. After the inner resistance increased by 20% at 1800s, the integrated voltage error gradually increases. After 800 seconds, it reaches the threshold and triggers the self-adaptation algorithm. In the scenario where the inner resistance increased by 50%, the larger error leads to the integrated error surpassing the threshold more rapidly, in about 300 seconds. Additionally, both the integrated error within 15 minutes and the real-time absolute error are higher. However, in both scenarios, the ECM in digital space dynamically self-adapts and once again matches the physical entity with the assistance of SaPSO algorithm. This is also evident in the lower subplot of Fig. 6, where the voltage error in both scenarios returns to within 0.5%. This demonstrates the ability of SaPSO algorithm to maintain accurate mapping between DT and the physical entity over long-term periods, even against dynamic operational conditions and the battery's inherent aging.

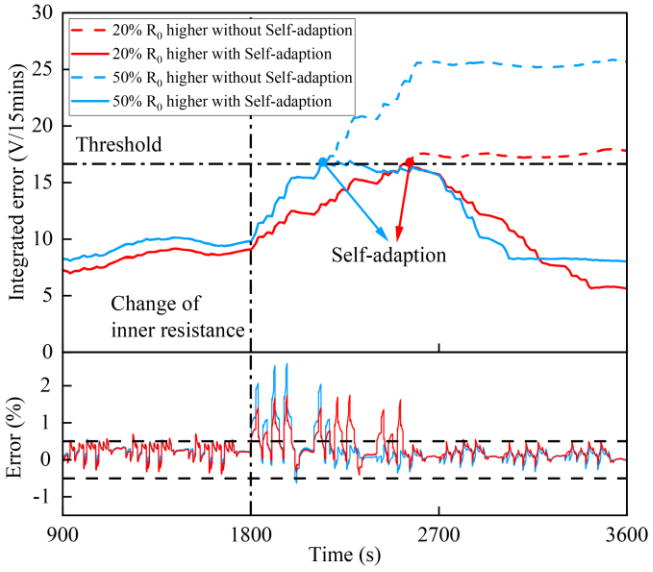

Fig. 6 Integrated voltage error in last 15 mins (upper) and the percentage voltage error between DT and physical entity with self-adaptation (lower).

Fig. 7 displays the validation results of one hundred repeated simulations for SaPSO robustness. It can be observed that after the change in internal resistance, SaPSO is activated within 900s, and the accuracy of the recalibrated DT model consistently falls within an acceptable range, despite variations in accuracy across each simulation.

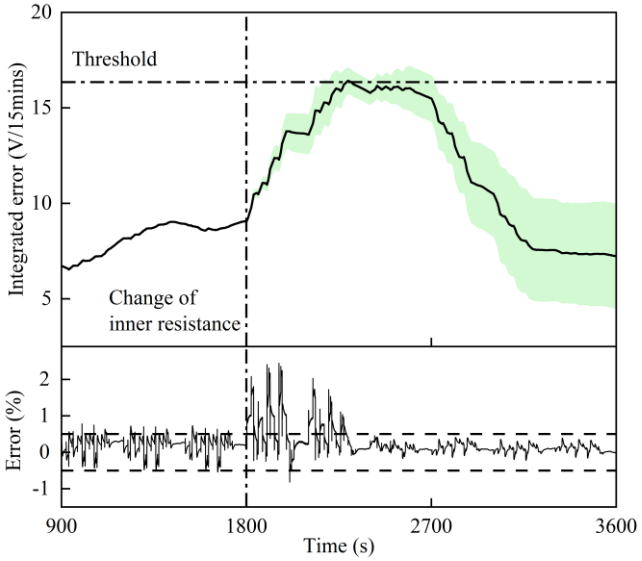

Fig. 7 Robustness analysis result of the propsoed SaPSO method. The black curves represent the average integrated voltage error (upper) and the percentage error (lower), and the shaded region illustrates the standard deviationof integrated error across 100 simulations.

B. *Results of monitoring and management*

Fig. 8 presents the estimated battery SOC using both the EKF and Ampere-hour integration methods. The lower subplot illustrates the absolute errors of the two methods. From the upper plot, it is evident that the EKF algorithm, which fuses data from both physical and digital spaces, exhibits higher accuracy. This is further supported by the absolute errors shown in the lower subplot. Additionally, the EKF method demonstrates a smaller root mean square error (0.41%) compared to the Ampere-hour integration method (1.24%).

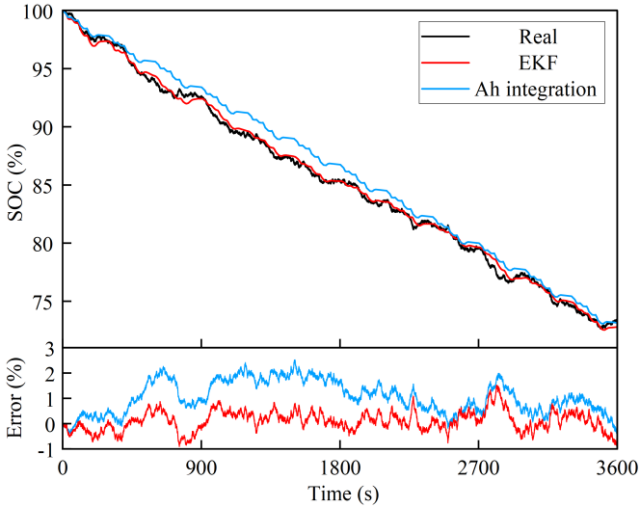

Fig. 8 Estimated SOC (upper) and estimation error (lower) using EKF and Ampere-hour integration methods.

The testing results for the first case, as depicted in the former 1800s in Fig. 9, illustrate that in the scenarios where there is a 10% initial SOC deviation, all the cells reach SOC equilibrium at 1150 seconds (high-dynamic) and 1166 seconds (low-dynamic), respectively. While the adjustment duration is

prolonged to 1410 seconds (high-dynamic) and 1421 seconds (low-dynamic) when confronted with a larger initial SOC deviation. Fundamentally, the employed MPC demonstrates similar performance in both high-dynamic and low-dynamic scenarios. However, a larger initial SOC deviation requires a longer adjustment period.

While facing the change of inner resistance at 1800s, scenarios A and C in Fig. 9 indicate that, the absence of self-adaptive algorithm causes a mismatch between physical entity and digital model. As a result, the control strategy provided by MPC loses effectiveness, resulting in an imbalance in battery SOC. In scenarios B and D, with the progression of charge and discharge processes, this imbalance is further intensified. With the implementation of the adaptive algorithm, SaPSO dynamically identifies the model parameters, enabling MPC to generate optimal control signals. Following a brief period of imbalance, the system gradually returns to equilibrium. The self-adaptation process, along with the comparison between scenarios with and without SaPSO, is clearly evident in the SOC variation subplots across various scenarios.

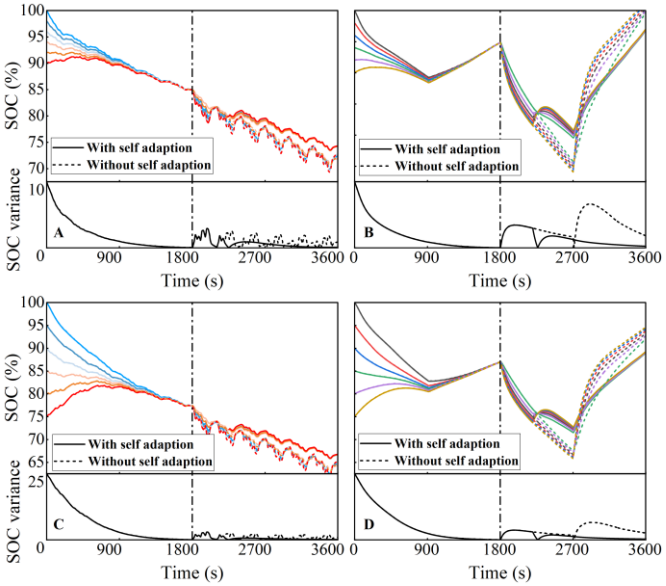

Fig. 9 Results of MPC-based SOC balancing for 6 batteries (represented by six distinct colors) connected in series under A: BBDST scenario with initial 10% SOC deviation, B: peak shaving scenario with initial 10% SOC deviation, C: BBDST scenario with initial 25% SOC deviation, D: peak shaving scenario with initial 25% SOC deviation.

Fig. 10 illustrates the results of extending the proposed SOC balancing strategy to the second case, totally 36 battery cells under both BBDST and peak-shaving scenarios. The black curves are the average SOC and the shaded area shows the SD of SOC deviation. The decrease in shadow indicates a reduction in SOC variance among battery cells. The SOC reaches equilibrium before 1800s, demonstrating the scalability of the proposed MPC-based SOC balancing method.

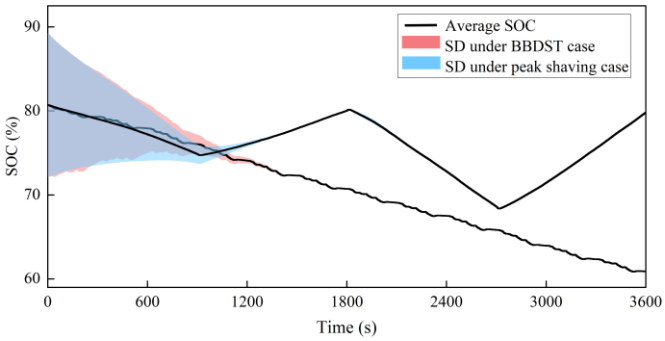

Fig. 10 SOC balancing results for larger-scaled battery pack.

IV. Conclusion

This paper presents the development of a self-adaptive DT-BMMS. In order to ensure the continuous matching between the digital model and the physical entity, a SaPSO-based parameter identification method is proposed in the modeling phase. Additionally, EKF is employed to accurately estimate the SOC of the battery, and MPC is applied to keep SOC balancing, enabling bi-directional information flow between the physical and digital spaces, thereby enhancing the overall performance of the battery system.

By introducing SaPSO, the long-term accurate mapping of the digital model to the physical entity is assured. Even facing changes in battery characteristic parameters due to aging or operating environment uncertainty, the adaptive algorithm can adjust model parameters in a short time. EKF provides users with accurate SOC monitoring information, demonstrating smaller root mean square error than the Ampere-hour integration method. Finally, MPC-based battery balancing management ensures SOC equalization for battery packs in both high-dynamic and low-dynamic scenarios in approximately 2 minutes. The proposed DT-BMMS addresses the challenge of the inability of MPC to provide optimal control signals when the battery model does not match the physical entity. It ensures that in uncertain environments, DT-BMMS can consistently and accurately monitor battery states and maintain battery SOC equilibrium.

For future work, the developed DT-BMMS will be calibrated in a laboratory setting, where a real battery system will replace the emulated battery to provide current and voltage measurement.

Acknowledgment

The work of Kun Fu was supported by the scholarship from China Scholarship Council (No. 202106220060). The work of Dr. Vedran S. Perić was supported by Deutsche Forschungsgemeinschaft (DFG) through the project “Optimal Operation of Integrated Low-Temperature Bidirectional Heat and Electric Grids (IntElHeat)” under Project number 450821044.

References

[1] R. Drath and A. Horch, "Industrie 4.0: Hit or Hype? [Industry Forum]," *IEEE Industrial Electronics Magazine*, vol. 8, no. 2, pp. 56-58, 2014, doi: 10.1109/MIE.2014.2312079.

[2] M. Dubarry, D. Howey, and B. Wu, "Enabling battery digital twins at the industrial scale," *Joule*, vol. 7, no. 6, pp. 1134-1144, 2023/06/21/ 2023, doi: https://doi.org/10.1016/j.joule.2023.05.005.
[3] M. W. Grieves, "Product lifecycle management: the new paradigm for enterprises," *International Journal of Product Development*, vol. 2, no. 1-2, pp. 71-84, 2005.
[4] E. J. Tuegel, A. R. Ingraffea, T. G. Eason, and S. M. Spottswood, "Reengineering Aircraft Structural Life Prediction Using a Digital Twin," *International Journal of Aerospace Engineering*, vol. 2011, p. 154798, 2011/10/23 2011, doi: 10.1155/2011/154798.
[5] C. Semeraro, H. Aljaghoub, M. A. Abdelkareem, A. H. Alami, M. Dassisti, and A. G. Olabi, "Guidelines for designing a digital twin for Li-ion battery: A reference methodology," *Energy*, vol. 284, p. 128699, 2023/12/01/ 2023, doi: https://doi.org/10.1016/j.energy.2023.128699.
[6] M. Naguib, P. Kollmeyer, and A. Emadi, "Lithium-Ion Battery Pack Robust State of Charge Estimation, Cell Inconsistency, and Balancing: Review," *IEEE Access*, vol. 9, pp. 50570-50582, 2021, doi: 10.1109/ACCESS.2021.3068776.
[7] H. Tang, Y. Wu, Y. Cai, F. Wang, Z. Lin, and Y. Pei, "Design of power lithium battery management system based on digital twin," *Journal of Energy Storage*, vol. 47, p. 103679, 2022/03/01/ 2022, doi: https://doi.org/10.1016/j.est.2021.103679.
[8] X. Qu, Y. Song, D. Liu, X. Cui, and Y. Peng, "Lithium-ion battery performance degradation evaluation in dynamic operating conditions based on a digital twin model," *Microelectronics Reliability*, vol. 114, p. 113857, 2020/11/01/ 2020, doi: https://doi.org/10.1016/j.microrel.2020.113857.
[9] N. G. Panwar, S. Singh, A. Garg, A. K. Gupta, and L. Gao, "Recent Advancements in Battery Management System for Li-Ion Batteries of Electric Vehicles: Future Role of Digital Twin, Cyber-Physical Systems, Battery Swapping Technology, and Nondestructive Testing," *Energy Technology*, vol. 9, no. 8, p. 2000984, 2021, doi: https://doi.org/10.1002/ente.202000984.
[10] J. Zhu, X. Cui, and W. Ni, "Model predictive control based control strategy for battery energy storage system integrated power plant meeting deep load peak shaving demand," *Journal of Energy Storage*, vol. 46, p. 103811, 2022/02/01/ 2022, doi: https://doi.org/10.1016/j.est.2021.103811.
[11] F. Naseri *et al.*, "Digital twin of electric vehicle battery systems: Comprehensive review of the use cases, requirements, and platforms," *Renewable and Sustainable Energy Reviews*, vol. 179, p. 113280, 2023/06/01/ 2023, doi: https://doi.org/10.1016/j.rser.2023.113280.
[12] Y. Wang, R. Xu, C. Zhou, X. Kang, and Z. Chen, "Digital twin and cloud-side-end collaboration for intelligent battery management system," *Journal of Manufacturing Systems*, vol. 62, pp. 124-134, 2022/01/01/ 2022, doi: https://doi.org/10.1016/j.jmsy.2021.11.006.
[13] W. Li, M. Rentemeister, J. Badeda, D. Jöst, D. Schulte, and D. U. Sauer, "Digital twin for battery systems: Cloud battery management system with online state-of-charge and state-of-health estimation," *Journal of Energy Storage*, vol. 30, p. 101557, 2020/08/01/ 2020, doi: https://doi.org/10.1016/j.est.2020.101557.
[14] C. Wang *et al.*, "Parameters identification of Thevenin model for lithium-ion batteries using self-adaptive Particle Swarm Optimization Differential Evolution algorithm to estimate state of charge," *Journal of Energy Storage*, vol. 44, p. 103244, 2021/12/01/ 2021, doi: https://doi.org/10.1016/j.est.2021.103244.
[15] Q. Ouyang *et al.*, "Module-Based Active Equalization for Battery Packs: A Two-Layer Model Predictive Control Strategy," *IEEE Transactions on Transportation Electrification*, vol. 8, no. 1, pp. 149-159, 2022, doi: 10.1109/TTE.2021.3095497.
[16] T.-E. Fan, S.-M. Liu, H. Yang, P.-H. Li, and B. Qu, "A fast active balancing strategy based on model predictive control for lithium-ion battery packs," *Energy*, vol. 279, p. 128028, 2023/09/15/ 2023, doi: https://doi.org/10.1016/j.energy.2023.128028.
[17] L. Zhou, D. Yang, X. Zeng, X. Zhang, and D. Song, "Multi-objective real-time energy management for series–parallel hybrid electric vehicles considering battery life," *Energy Conversion and Management*, vol. 290, p. 117234, 2023/08/15/ 2023, doi: https://doi.org/10.1016/j.enconman.2023.117234.
[18] G. Aurilio *et al.*, "A battery equivalent-circuit model and an advanced technique for parameter estimation," in *2015 IEEE International Instrumentation and Measurement Technology Conference (I2MTC) Proceedings*, 11-14 May 2015 2015, pp. 1705-1710, doi: 10.1109/I2MTC.2015.7151537.
[19] W. Wang, J. Wang, J. Tian, J. Lu, and R. Xiong, "Application of Digital Twin in Smart Battery Management Systems," *Chinese Journal of Mechanical Engineering*, vol. 34, no. 1, p. 57, 2021/06/09 2021, doi: 10.1186/s10033-021-00577-0.
[20] X. Du *et al.*, "An information appraisal procedure: Endows reliable online parameter identification to lithium-ion battery model," *IEEE Transactions on Industrial Electronics*, vol. 69, no. 6, pp. 5889-5899, 2021.
[21] J. Kennedy, "Particle Swarm Optimization," in *Encyclopedia of Machine Learning*, C. Sammut and G. I. Webb Eds. Boston, MA: Springer US, 2010, pp. 760-766.
[22] "European Energy Exchange (EPEX)." http://www.epexspot.com/en/. (accessed on 05 Feb. 2024).
[23] R. Faragher, "Understanding the Basis of the Kalman Filter Via a Simple and Intuitive Derivation [Lecture Notes]," *IEEE Signal Processing Magazine*, vol. 29, no. 5, pp. 128-132, 2012, doi: 10.1109/MSP.2012.2203621.
[24] A. Thelen *et al.*, "A comprehensive review of digital twin — part 1: modeling and twinning enabling technologies," *Structural and Multidisciplinary Optimization*, vol. 65, no. 12, p. 354, 2022/11/28 2022, doi: 10.1007/s00158-022-03425-4.
[25] Eberhart and S. Yuhui, "Particle swarm optimization: developments, applications and resources," in *Proceedings of the 2001 Congress on Evolutionary Computation (IEEE Cat. No.01TH8546)*, 27-30 May 2001 2001, vol. 1, pp. 81-86 vol. 1, doi: 10.1109/CEC.2001.934374.
[26] M. Clerc, "The swarm and the queen: towards a deterministic and adaptive particle swarm optimization," in *Proceedings of the 1999 Congress on Evolutionary Computation-CEC99 (Cat. No. 99TH8406)*, 6-9 July 1999 1999, vol. 3, pp. 1951-1957 Vol. 3, doi: 10.1109/CEC.1999.785513.
[27] B. G. Carkhuff, P. A. Demirev, and R. Srinivasan, "Impedance-Based Battery Management System for Safety Monitoring of Lithium-Ion Batteries," *IEEE Transactions on Industrial Electronics*, vol. 65, no. 8, pp. 6497-6504, 2018, doi: 10.1109/TIE.2017.2786199.
[28] Y.-S. Duh *et al.*, "Characterization on thermal runaway of commercial 18650 lithium-ion batteries used in electric vehicles: A review," *Journal of Energy Storage*, vol. 41, p. 102888, 2021/09/01/ 2021, doi: https://doi.org/10.1016/j.est.2021.102888.
[29] F. C. Sun, X. F. Meng, C. Lin, and Z. P. Wang, "Dynamic stress test profile of power battery for electric vehicle," vol. 30, pp. 297-301, 03/01 2010.
[30] Y. Guo, J. Cai, Y. Liao, J. Hu, and X. Zhou, "Insight into fast charging/discharging aging mechanism and degradation-safety analytics of 18650 lithium-ion batteries," *Journal of Energy Storage*, vol. 72, p. 108331, 2023/11/15/ 2023, doi: https://doi.org/10.1016/j.est.2023.108331.